JOURNAL OF COMPUTATIONAL PHYSICS 118, 229–241 (1995)

An Adaptive TVD Limiter*

YIH NEN JENG† AND UON JAN PAYNE

Institute of Aeronautics and Astronautics, National Cheng Kung University, 70101, Tainan, Taiwan, Republic of China

Received June 15, 1992; revised September 6, 1994

An adaptive TVD limiter, based on a limiter approximating the upper boundary of the TVD range and that of the third-order upwind TVD scheme, is developed in this work. The limiter switches to the comprressive limiter near a discontinuity, to the third-order TVD scheme's limiter in the smooth region, and to a weighted averaged scheme in the transition region between smooth and high gradient solutions. Numerical experiments show that the proposed scheme works very well for one-dimensional scalar equation problems but becomes less effective in one- and two-dimensional Euler equation problems. Further study is required for the two-dimensional scalar equation problems.

INTRODUCTION

Total variational diminishing (TVD) schemes [1–5] are one of the most important schemes in solving hyperbolic conservation laws. For aerodynamic problems, TVD schemes have many successful applications for use with the Euler and Navier–Stokes equations [3]. Around the time that Harten [1, 2] proposed the sufficient conditions defining TVD schemes, many limiter functions [3–5], each having a different effect on the solution, were developed and subsequently examined in detail. Unfortunately, many schemes have drawbacks [4, 5], such as the Roe minmod limiter [1, 2, 4], which tends to smear discontinuities, and the Roe superbee limiter [4], which sometimes compresses a smooth solution into discontinuity. In general, most schemes smear the linear contact discontinuity without limit. For convenience, we say that a TVD limiter, such as the superbee limiter, is a compressive limiter, and that a TVD limiter, such as the minmod limiter, is a diffusive limiter. From the point of view of solving hyperbolic conservation laws, it is therefore advantageous to search for new limiters that retain smoothness in the smooth solution region while compressing discontinuities and high gradient regions, especially around a linear discontinuity.

Generally speaking, a TVD limiter often contains a switch that changes the scheme from one to another when some critical conditions are present. It is intuitive to enlarge the function of the switch so that, in addition to ensuring the satisfaction of the Harten TVD conditions, the TVD scheme can also retain solution smoothness and discontinuity. Therefore, a solution adaptive limiter, which is a combination of diffusive and compressive TVD limiters, is the main concern of the present study.

Sweby [6] modified the Lax–Wendroff scheme by adding a limiter, φ, and identified the TVD range of the limited scheme for a linear scalar equation. Note that in order to account for the nonlinear effect and to be independent of the Courant number, this TVD range was defined conservatively. In the same paper, numerical results showed that the compressive character of the examined TVD schemes was proportional to the magnitude of φ. As a consequence, the compressive nature of a TVD scheme needs to be restricted to a certain extent. In fact, Roe and Baines [4, 7, 8, 28] had already found the upper limiter of the TVD range for the linear scalar equation (they called it the monotonicity constraint), whose associated $\varphi_{\max}$ depends on the CFL number and is larger than that of Sweby's work.

In our previous studies [9–11], we had proposed two TVD limiters which were more compressive than the superbee limiter. Unfortunately, their resolution of linear discontinuity is much less impressive than that of the Harten ENO scheme with subcell-resolution [12, 13]. Apparently, the incompleteness of the limiter's switching function is responsible for such shortcomings. Therefore, in order to enhance the switching function, the "spirit" of Harten's ENO scheme will be incorporated in this study.

ANALYSIS

In order to design an adaptive TVD limiter, we need information on the upper limit of the TVD range. Roe and Baines [4, 7, 8, 28] had already found the limit for the linear scalar wave equation in terms of the monotone condition. For the sake of completeness, this study will follow Sweby's formulation to revisit the limit for the following nonlinear scalar wave equation,

$$u_t + f(u)_x = 0, \tag{1}$$

where u is a dependent variable, $f(u)$ is the nonlinear flux, x is the spatial coordinate, and t denotes time. Without loss of generality, the modified Lax–Wendroff scheme (equipped with a limiter) can be written as

* Supported by FDID Grant 79-F008.

† To whom correspondence should be addressed.

0021-9991/95 $6.00

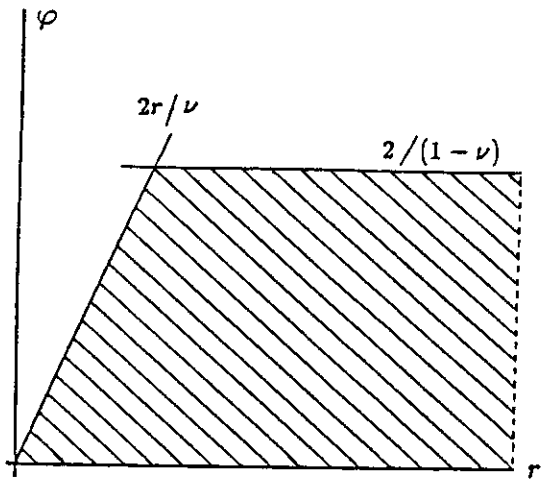

FIG. 1. The TVD ranges of Eqs. (18) and (19) on the (φ, r) plane.

$$u_i^{n+1} = u_i^n - \lambda(h_{i+1/2}^{LW} - h_{i-1/2}^{LW}), \quad \lambda = \Delta t/\Delta x \tag{2}$$

$$h_{i+1/2}^{LW} = \tfrac{1}{2}[f_{i+1} + f_i - |a_{i+1/2}|\,\Delta_{i+1/2}u + (1 - \nu_{i+1/2})(\varphi_{i+1/2}^{+}a_{i+1/2}^{+} - \varphi_{i+1/2}^{-}a_{i+1/2}^{-})\,\Delta_{i+1/2}u]$$

$$\Delta_{i+1/2}(\ ) = (\ )_{i+1} - (\ )_i$$

$$a_{i+1/2} = \Delta_{i+1/2}f/\Delta_{i+1/2}u, \quad u_i \neq u_{i+1}$$

$$= \frac{\partial f}{\partial u}, \quad u_i = u_{i+1}$$

$$\nu_{i+1/2} = |a_{i+1/2}|\,\Delta t/\Delta x \leq 1$$

$$a_{i+1/2}^{\pm} = \tfrac{1}{2}(a_{i+1/2} \pm |a_{i+1/2}|),$$

where the limiter $\varphi_{i+1/2}^{\pm}$ is obviously an anti-diffusion term, and $\varphi_{i+1/2}^{\pm} = 1$ for the original L-W scheme. Note that all the TVD schemes based on the slope limiter (not in form of $\varphi\,\Delta f$) can be expressed in this form with a suitable φ after proper transformation [9].

Following the procedure for finding the TVD condition outlined in Refs. [1, 2],

$$\mathrm{TV}[u^{n+1}] \leq \mathrm{TV}[u^n] \tag{3}$$

$$\mathrm{TV}[u^n] = \sum_i |\Delta_{i+1/2}u^n|, \tag{4}$$

Eq. (2) can be rewritten as

$$u_i^{n+1} = u_i^n + C_{i+1/2}^{+}\,\Delta_{i+1/2}u - C_{i-1/2}^{-}\,\Delta_{i-1/2}u \tag{5}$$

$$C_{i+1/2}^{+} = \frac{\lambda}{2}\{[2 - (1 - \nu_{i+1/2})\varphi_{i+1/2}^{-}]|a_{i+1/2}^{-}| + (1 - \nu_{i-1/2})\varphi_{i-1/2}^{-}|a_{i-1/2}^{-}|/r_{i-1/2}^{+}\}$$

$$C_{i-1/2}^{-} = \frac{\lambda}{2}\{[2 - (1 - \nu_{i-1/2})\varphi_{i-1/2}^{+}]|a_{i-1/2}^{+}| + (1 - \nu_{i+1/2})\varphi_{i+1/2}^{+}|a_{i+1/2}^{+}|/r_{i+1/2}^{-}\}$$

$$r_{i+1/2}^{\pm} = \Delta_{i+1/2\pm1}u/\Delta_{i+1/2}u,$$

where the variation ratios, $r^{\pm}$, are the slope ratios. The sufficient conditions of scheme, Eq. (5), for satisfying the TVD condition, Eq. (3), are

$$C_{i+1/2}^{\pm} \geq 0 \tag{6}$$

$$C_{i+1/2}^{+} + C_{i+1/2}^{-} \leq 1. \tag{7}$$

If one considers all the possible sign arrangements of $a_{i-1/2}$, $a_{i+1/2}$, and $a_{i+3/2}$, the TVD range of the limiter, $\varphi_{i+1/2}^{\pm}$, can be found. The non-negative TVD condition, Eq. (6), is automatically satisfied, if for all i

$$\varphi_{i+1/2}^{\pm} \leq \frac{2}{1 - \nu_{i+1/2}} \tag{8}$$

$$\frac{\varphi_{i+3/2}^{\pm}}{r_{i+3/2}^{-}} \geq 0, \tag{9}$$

provided that $\nu_{i+1/2} \leq 1$. It can be proved that Eq. (7) can be satisfied if the following conditions are fulfilled:

$$0 \leq \frac{\nu_{i+1/2}}{2}[2 - (1 - \nu_{i+1/2})\varphi_{i+1/2}^{+}] + \frac{\nu_{i+3/2}}{2}(1 - \nu_{i+3/2})\frac{\varphi_{i+3/2}^{+}}{r_{i+3/2}^{-}} \leq 1. \tag{10}$$

By introducing two arbitrary constants, say α and β, those

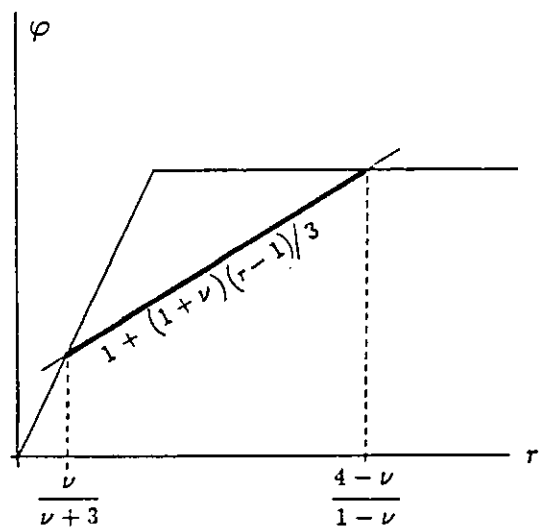

FIG. 2. The limiter function corresponding to the third-order upwind scheme which satisfies the TVD condition in the range of $\nu/(\nu + 3) \leq r \leq (4 - \nu)/(1 - \nu)$.

constraints sufficient to satisfy the inequality of Eq. (6) can be denoted as

$$\alpha \leq \frac{\nu_{i+3/2}}{2}(1-\nu_{i+3/2})\frac{\varphi^{+}_{i+3/2}}{r^{-}_{i+3/2}} \leq \beta \tag{11}$$

$$-\alpha \leq \frac{\nu_{i+1/2}}{2}[2-(1-\nu_{i+1/2})\varphi^{+}_{i+1/2}] \leq 1-\beta. \tag{12}$$

It is obvious, from Eqs. (9) and (11), that $\alpha = 0$ and $\beta \geq 0$. With this in mind, then, Eqs. (11) and (12) become

$$0 \leq \frac{\varphi^{+}_{i+3/2}}{r^{-}_{i+3/2}} \leq \frac{2\beta}{\nu_{i+3/2}(1-\nu_{i+1/2})} \tag{13}$$

$$\left[\frac{2(\beta-1)}{\nu_{i+1/2}}+2\right]\Big/(1-\nu_{i+1/2}) \leq \varphi^{+}_{i+1/2} \leq \frac{2}{1-\nu_{i+1/2}}. \tag{14}$$

Since φ is an anti-diffusion term, a larger value of φ associates to a less diffusive scheme (and a more compressive limiter) [6]. In order to search for a potential TVD limiter more compressive than the superbee limiter, a larger β value is preferrable. On the other hand, if $\varphi^{+}_{i+1/2} = 0$ is employed, the scheme becomes a first-order upwind scheme (a very diffusive TVD scheme). Therefore, it seems reasonable to take the lower limit of Eq. (14) to be zero, so that β takes the value

$$\beta = 1-\nu_{i+1/2}. \tag{15}$$

Subsequently, Eqs. (13) and (14) can be rewritten as

$$0 \leq \frac{\varphi^{+}_{i+3/2}}{r^{-}_{i+3/2}} \leq \frac{2(1-\nu_{i+1/2})}{\nu_{i+3/2}(1-\nu_{i+3/2})}$$

$$0 \leq \varphi^{+}_{i+1/2} \leq \frac{2}{1-\nu_{i+1/2}}. \tag{16}$$

Similarly, we can get

$$0 \leq \frac{\varphi^{-}_{i-1/2}}{r^{+}_{i-1/2}} \leq \frac{2(1-\nu_{i+1/2})}{\nu_{i-1/2}(1-\nu_{i-1/2})}$$

$$0 \leq \varphi^{-}_{i+1/2} \leq \frac{2}{1-\nu_{i+1/2}}. \tag{17}$$

Consequently, the TVD range of $\varphi^{\pm}_{i+1/2}$ is

$$0 \leq \varphi^{\pm}_{i+1/2} \leq \min\left[\frac{2}{1-\nu_{i+1/2}}, \frac{2r^{\mp}_{i+1/2}(1-\nu_{i+1/2\mp1})}{\nu_{i+1/2}(1-\nu_{i+1/2})}\right], \quad \text{for } r^{\mp}_{i+1/2} > 0 \tag{18a}$$

$$\varphi^{\pm}_{i+1/2} = 0, \qquad \text{for } r^{\mp}_{i+1/2} \leq 0. \tag{18b}$$

For a linear equation with constant wave speed, Eq. (18a) reduces to the Roe and Baines monotonicity constraint [4, 7, 8]

$$0 \leq \varphi^{+}_{i+1/2} \leq \min\left[\frac{2}{1-\nu}, \frac{2r^{\mp}_{i+1/2}}{\nu}\right], \quad r^{\mp}_{i+1/2} > 0, \tag{19}$$

where $\nu = \nu_{i+1/2} \leq 1$ is the CFL condition. For the sake of clarity, these conditions are shown in Fig. 1. Note that this figure is equivalent to the universal limiter constraints of Leonard (Fig. A2 in Ref. [14] and Fig. 2 in Ref. [15]). Now, a TVD limiter more compressive than the superbee limiter can be designed, whose $\varphi - r$ relation closely approximates the upper boundary of the TVD range defined by either Eq. (18) or (19). Intuitively, it seems that a TVD limiter that is more compressive than the superbee limiter would have undesirable overcompressive characteristics, which may explain why researchers have not paid attention to this TVD region before [4, 7, 8].

In Refs. [9–11], we introduced the idea of an adaptive TVD limiter incorporating not only a diffusive TVD limiter for use in the regions of smooth solution, but which could also switch to a compressive TVD limiter at appropriate locations. Obviously, the question to be addressed here relates to location. Where should the compressive limiter be switched on, if it is to be switched on at all? Our experience [9–11] shows that the following rules are helpful in making this decision:

(1) A compressive limiter should be switched around a discontinuity, such as either $r^{\pm}_{i+1/2} \to 0$ or $r^{\pm}_{i+1/2} \to \infty$.

(2) A high order accurate limiter is preferred in smooth regions with $r^{\pm}_{i+1/2}$ being located around unity.

In fact, these rules are not new. Rule (1) is similar to the first two properties of the Roe B-function [4], while rule (2) is similar to the third property of the B-function.

However, the compressive character of the TVD schemes (designed in Refs. [9–11] and based on these rules) does not give impressive resolutions for linear discontinuities. The authors suspect that the compressive character of the aforementioned schemes can not be further improved by defining a limiter function in the form $\varphi^{\pm}_{i+1/2} = \varphi^{\pm}_{i+1/2}(r^{\mp}_{i+1/2})$. In fact, even if $r^{\pm}_{i+1/2} \sim 1$ was found, one could not determine from the scheme whether or not $r^{\mp}_{i+1/2\pm1} \to 0$ or ∞. In other words, the

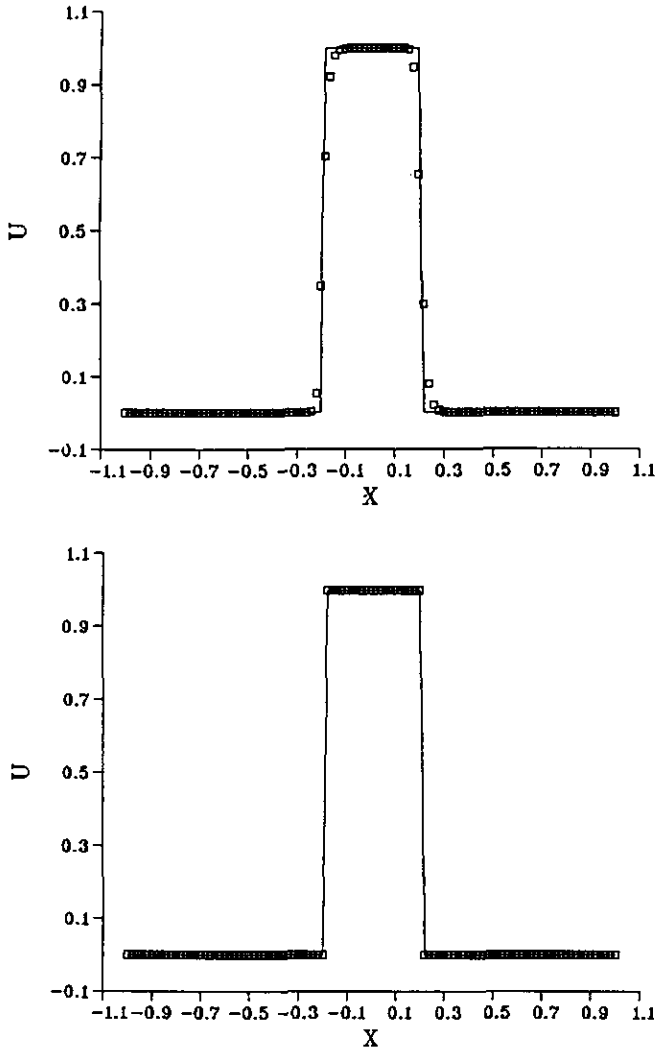

FIG. 3. The solution to the square wave problem, using the initial conditions of Eq. (37a), found by (a) the superbee TVD scheme, (b) the present TVD scheme, Eqs. (23)–(25).

classical definitions of a limiter are not clever enough to detect whether or not a control surface is located around a discontinuity.

Harten's subcell resolution scheme [12] and Shu and Osher's efficient implementation [13], based on the ENO scheme, considered all the information around the control surface of $x_{i+1/2}$, so that no information was missed. Consequently, their schemes could be perfected for capturing discontinuities. By virtue of their success, we would like to propose an additional rule:

(3) If $r^-_{i+1/2} \sim 1$ for $a_{i+1/2} > 0$, and if either $r^-_{i+3/2} \to \infty$ or $r^-_{i+3/2} \to 0$, a compressive limiter is preferred.

These rules can now be employed in order to define a new adaptive TVD limiter. First, consider the following high-order scheme suitable for smooth solution regions. It can be shown that once $\varphi^\pm$ satisfies

$$\frac{\varphi^\pm_{i\pm1/2} - 1}{r^\mp_{i\pm1} - 1} = \frac{1 + \nu_{i\pm1/2}}{3} \tag{20}$$

the modified Lax–Wendroff scheme, Eq. (2), becomes a third-order scheme. Moreover, it can also be shown that, for the linear case with constant wave speed, the third-order scheme satisfies TVD conditions within the region

$$\frac{\nu}{\nu + 3} \leq r^\pm \leq \frac{4 - \nu}{1 - \nu}. \tag{21}$$

By virtue of rule (2), therefore, the third-order upwind scheme of Eq. (20) can be employed within this range of r, as shown in Fig. 2.

In order to determine the region in which the compressive limiter should be switched on, either the Harten criterion [12] or the Shu and Osher criterion [13] is a good candidate. In this study, the latter criterion is employed, resulting in the identification of a discontinuity at the critical interval $I(x_{i-1/2}, x_{i+1/2})$, where

$$\begin{aligned} &s_i \geq s_{i+1} \quad \text{and} \quad s_i \geq s_{i-1} \\ &s_i = |m[(u_{i+1} - u_i), (u_i - u_{i-1})]|, \end{aligned} \tag{22}$$

where $m(\cdot, \cdot)$ denotes the minmod function. Note that this criterion satisfies rules (1) and (3) simultaneously. In summary, for positive wave speed at the i-cell, the limiter takes the form

$$\begin{aligned} \varphi^-_{i+1/2} &= 0, && \text{if } r^-_{i+1/2} \leq 0 \\ &= \min\left[\phi_{i+1/2}, \frac{2r^-_{i+1/2}}{\nu_{i+1/2}}, \frac{2}{1 - \nu_{i+1/2}}\right], && \text{if } r^-_{i+1/2} > 0, \end{aligned} \tag{23}$$

where

$$\phi_{i+1/2} = \frac{2}{1 - \nu_{i+1/2}}, \qquad \text{if Eq. (22) is satisfied} \tag{24}$$

$$= 1 + \frac{(1 + \nu_{i+1/2})(r^-_{i+1/2} - 1)}{3}, \quad \text{otherwise.} \tag{25}$$

Equations (23)–(24) state that, if a discontinuity exists in the ith cell, then the upper boundary of the TVD region should be chosen as the TVD limiter, regardless of whether $r^\pm \sim 1$ or not. However, if no discontinuity exists, then a third-order scheme (say Eq. (25)) should be employed.

Note that the subcell resolution schemes of Ref. [12–13] are constructed on the basis of the ENO scheme. Although the critical interval defined in Eq. (22) may only be a smooth inflection point, the integration procedure for such schemes can

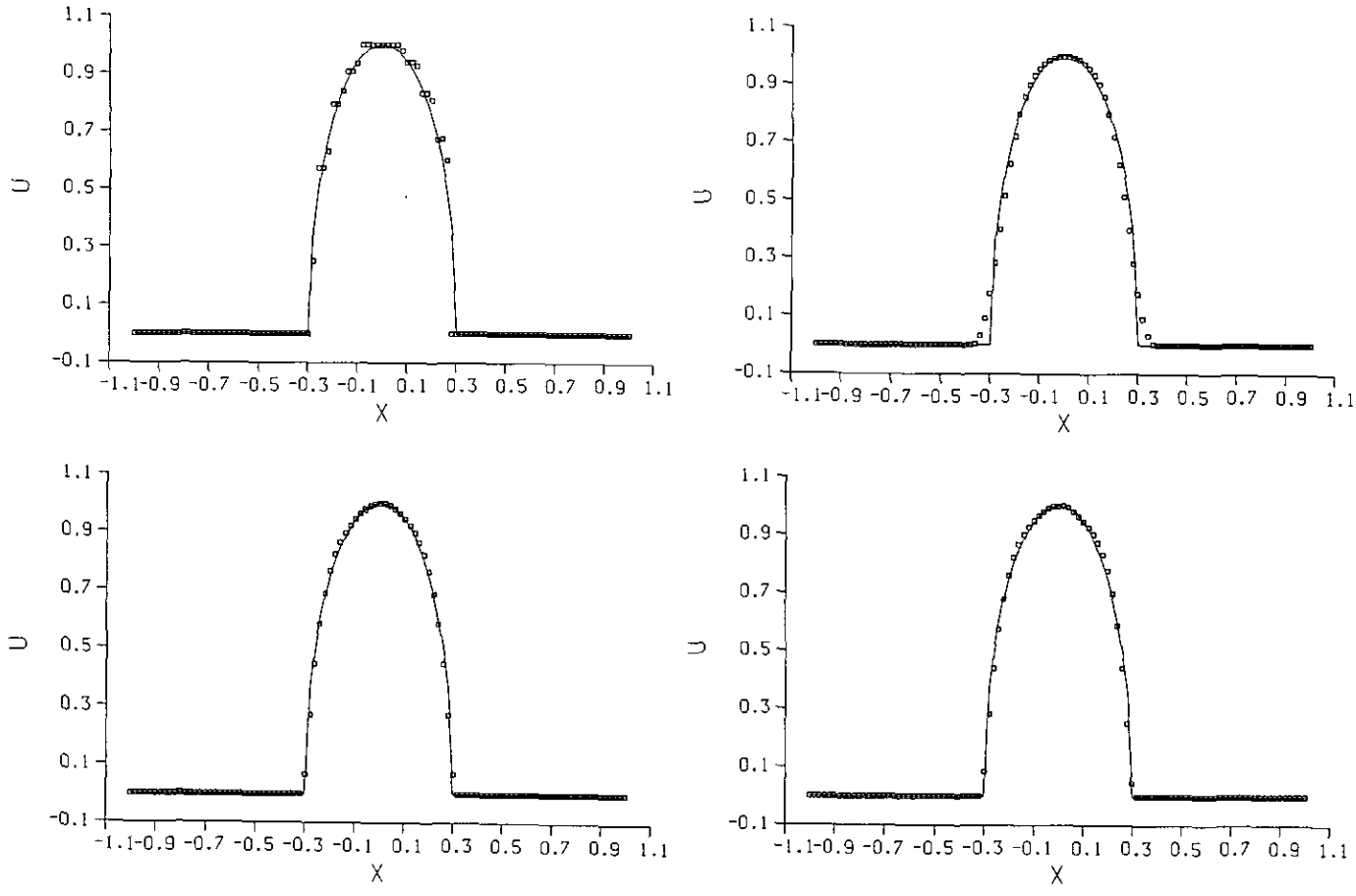

FIG. 4. The solution to the problem using the initial conditions of Eq. (37b), found by (a) the present TVD scheme using Eqs. (23)–(25), (b) the third-order upwind TVD scheme, (c) the adaptive TVD scheme, Eqs. (23), (26)–(28), and $K = 1$, $\omega_o = 0.1$, $\Delta\omega = 0.05$, and $\nu = 0.5$; (d) the adaptive TVD scheme, Eqs. (23), (26)–(28), and $K = 1$, $\omega_o = 0.1$, $\Delta\omega = 0.05$, and $\nu = 0.4$.

easily recover the necessary smoothness. However, since the present method does not contain any smoothing process, the method proposed in Eqs. (22)–(25) might compress a smooth solution into a high gradient solution, if the discontinuity switch is interpreted incorrectly. In order to avoid such a possibility, the magnitude $\Delta u_i^n/\Delta u_{\max}^n$ and the slope ratios $r_{i-1/2}^+$ and $r_{i+3/2}^-$ are employed to decide in the smooth region. Therefore, a better expression for the $\phi_{i+1/2}$ term of Eqs. (24)–(25) is: if Eq. (22) is satisfied and $\max[|\Delta_{i-1/2}u^n|, |\Delta_{i+1/2}u^n|, |\Delta_{i+3/2}u^n|]$, then

$$\phi_{i+1/2} = \phi_1, \quad \text{if } r_{i+3/2}^- > \frac{4 - \nu_{i+1/2}}{1 - \nu_{i+1/2}}, \; r_{i-1/2}^+ < \frac{\nu_{i+1/2}}{3 + \nu_{i+1/2}} \tag{26}$$

$$= (1 - \omega)\phi_1 + \omega\phi_2, \quad \text{if } r_{i+3/2}^- > \frac{4 - \nu_{i+1/2}}{1 - \nu_{i+1/2}} \text{ or } r_{i-1/2}^+ < \frac{\nu_{i+1/2}}{3 + \nu_{i+1/2}}; \tag{27}$$

otherwise,

$$\phi_{i+1/2} = \phi_1, \quad \text{if Eq. (22) is not satisfied, or } \max[|\Delta_{i-1/2}u^n|, |\Delta_{i+1/2}u^n|, |\Delta_{i+3/2}u^n|] \le K|\Delta_{i+1/2}u^n|_{\text{mean}} \tag{28}$$

$$\phi_1 = 1 + \frac{(1 + \nu_{i+1/2})(r_{i+1/2}^- - 1)}{3}$$

$$\phi_2 = \text{Min}\left[\frac{2}{1 - \nu_{i+1/2}}, \frac{2r_{i+1/2}^-}{\nu_{i+1/2}}\right]$$

$$\omega = \omega_0 + \Delta\omega \frac{\max[|\Delta_{i-1/2}u^n|, |\Delta_{i+1/2}u^n|, |\Delta_{i+3/2}u^n|] \le K|\Delta_{i+1/2}u^n|_{\text{mean}}}{|\Delta_{i+1/2}u^n|_{\max} - K|\Delta_{i+1/2}u^n|_{\text{mean}}},$$

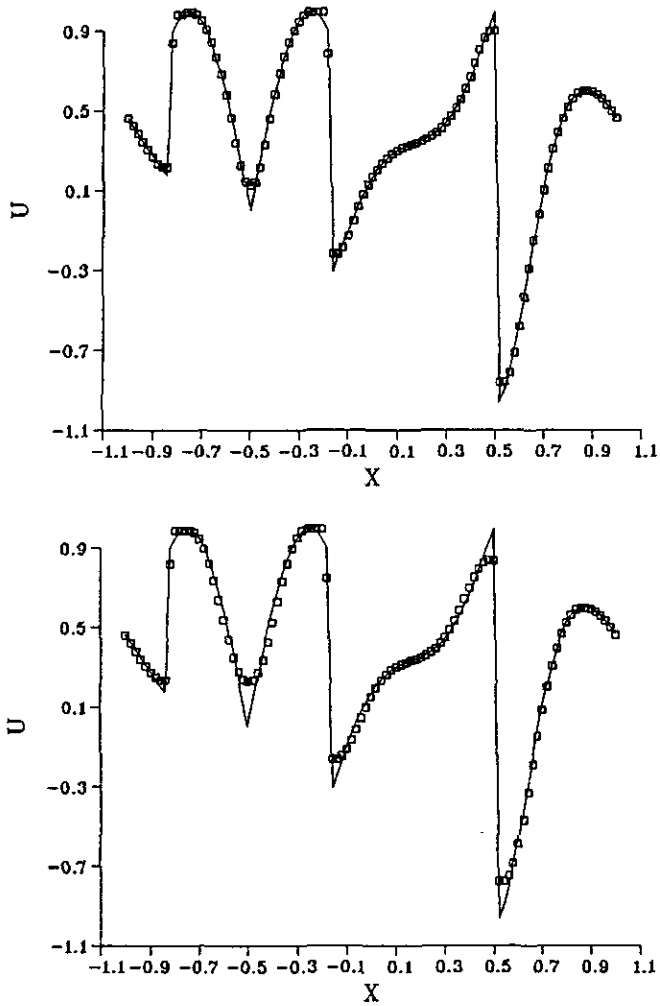

FIG. 5. The proposed TVD scheme's (Eqs. (23), (26), (28)) solution to the third problem, using the initial conditions of Eq. (37c) at (a) $t = 2$, with $\nu = 0.8$, and 100 uniform grid points; (b) $t = 20$, with $\nu = 0.8$, and 100 uniform grid points.

where K (ranged from 1 to 3), ω_o, and $\Delta\omega$ are user-specified constants. The magnitude $|\Delta u^n|_{\text{mean}}$ is introduced to avoid having a smooth solution considered to be a discontinuity. The modification in Eq. (26) states that the flux at $x = x_{i+1/2}$ around a discontinuity should be equipped with the compressive limiter only if $|\Delta_{i+3/2}u^n| \ll |\Delta_{i+1/2}u^n|$ and $|\Delta_{i-3/2}u^n| \ll |\Delta_{i-1/2}u^n|$. Although this works very well in the examples given in the present study, such a modification might still consider a smooth inflection point to be a shock.[1] To avoid such a setback, one may tune the criteria to be $r^-_{i+3/2} > k_1(4 - \nu_{i+1/2})/(1 - \nu_{i+1/2})$ and $r^-_{i-1/2} < (1/k_2)(\nu_{i+1/2})/(3 + \nu_{i+1/2})$, where k_1 and k_2 are scaling constants. The modification of Eq. (27) is suitable for the transition region between smooth and high gradient solutions.

[1] The authors are grateful to one of the referees who pointed out this fact.

Across from a local extreme point, most TVD schemes are reduced to first-order accuracy because of Eq. (18b). Such a reduction frequently leads to the so-called clipping effect around an extreme point. In order to remedy this problem, Lenord and Niknafs [15] proposed an extreme point corrector, and this idea was added to the system equation case by Jeng *et al.* [11, 16]. The corrector of Ref. [15] identifies an extreme point as a numerical oscillation whenever the second-order differences change sign across from the point. In order to avoid numerical oscillation around a discontinuity, the extension of Refs. [11, 16] adds an asymmetric factor which considers extreme points next to a discontinuity as numerical oscillation. Once an extreme point is recognized as a numerical oscillation, the TVD limiter is preserved. Otherwise, the limiter is switched off for several neighboring control surfaces. In this study, the modified extremum corrector is employed.

As the proposed TVD limiter is applied to two-dimensional scalar wave equations, the directional operator splitting approximation is employed [1, 4, 17]. For the one-dimensional Euler equation problem, the Roe approximate Riemann solver [18] and the Coakley eigenvalue splitting approximation [19] are employed. Because the above two methods are simplified forms of the following two-dimensional Euler equations problem, they are not shown here. It is easily shown that the Coakely splitting introduces intrinsic dissipation at the sonic point [9, 20]. Although this is not proven to be an E-scheme, our numerical experiments show that the expansion shock has yet to be found.

For two-dimensional problems, the two-dimensional Euler equations in conservative form are

$$\frac{\partial \mathbf{U}}{\partial t} + \frac{\partial \mathbf{F}(\mathbf{U})}{\partial x} + \frac{\partial \mathbf{G}(\mathbf{U})}{\partial y} = 0, \tag{29a}$$

where

$$\mathbf{U} = \begin{bmatrix} \rho \\ \rho u \\ \rho v \\ e \end{bmatrix}, \quad \mathbf{F} = \begin{bmatrix} \rho u \\ \rho u^2 + p \\ \rho uv \\ u(e + p) \end{bmatrix}, \quad \mathbf{G} = \begin{bmatrix} \rho v \\ \rho uv \\ \rho v^2 + p \\ v(e + p) \end{bmatrix} \tag{29b}$$

in which ρ is the density, u and v are the velocity components in x- and y-directions, respectively, and p is the pressure. The total energy per unit volume e is related to p by the equation of state for a perfect gas,

$$p = (\gamma - 1)[e - \rho(u^2 + v^2)/2]. \tag{29c}$$

Define

$$\hat{\mathbf{F}} = \Delta y \mathbf{F}, \quad \hat{\mathbf{G}} = \Delta x \mathbf{G}$$

$$\hat{\mathbf{U}} = \frac{1}{J}\mathbf{U}, \quad \hat{\mathbf{A}} = \frac{\partial \hat{\mathbf{F}}}{\partial \hat{\mathbf{U}}}, \quad \hat{\mathbf{B}} = \frac{\partial \hat{\mathbf{G}}}{\partial \hat{\mathbf{U}}}, \tag{30}$$

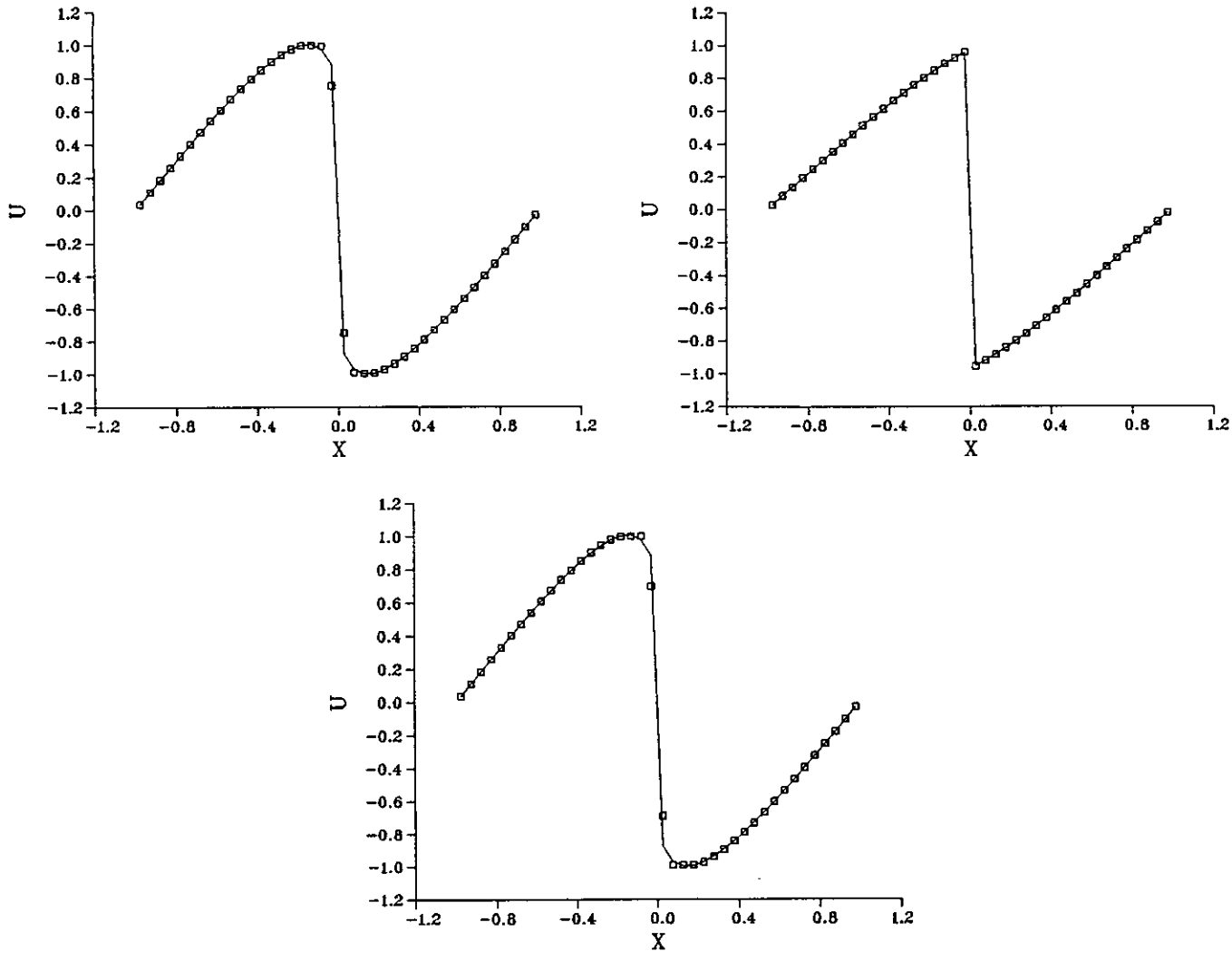

FIG. 6. The proposed TVD scheme's (eqs. (23), (26), (28)) solution to the Burgers equation, using the initial conditions of Eq. (38) (a) before the formation of the shock wave, $\nu = 0.8$; (b) after the formation of the shock wave, $\nu = 0.8$; (c) after the formation of the shock wave, $\nu = 0.2$.

where $1/J = \Delta x\, \Delta y$ is area of the cell. Let eigenvalues of $\hat{\mathbf{A}}$, $\hat{\mathbf{B}}$ be a^l, $\hat{a}^l$, respectively, where $l = 1, 2, 3, 4$. Denote $\tilde{\mathbf{R}}$ and $\hat{\mathbf{R}}$ as the matrices whose columns are right eigenvectors of $\hat{\mathbf{A}}$ and $\hat{\mathbf{B}}$, respectively, and $\tilde{\mathbf{R}}^{-1}$ and $\hat{\mathbf{R}}^{-1}$ are their corresponding inverse matrices. After employing the Roe approximate Riemann solver and the Coakley eigenvalue splitting, the one-parameter family of TVD schemes for Eq. (29) on the Cartesian grid system become

$$\begin{aligned}\hat{\mathbf{U}}_{j,k}^{n+1} &+ \Delta t\, \phi[\tilde{\mathbf{F}}_{j+1/2,k}^{n+1} - \tilde{\mathbf{F}}_{j-1/2,k}^{n+1}] \\ &+ \Delta t\, \phi[\tilde{\mathbf{G}}_{j,k+1/2}^{n+1} - \tilde{\mathbf{G}}_{j,k-1/2}^{n+1}] \\ &= \hat{\mathbf{U}}_{j,k}^{n} - \Delta t(1-\phi)[\tilde{\mathbf{F}}_{j+1/2,k}^{n} - \tilde{\mathbf{F}}_{j-1/2,k}^{n}] \\ &- \Delta t(1-\phi)[\tilde{\mathbf{G}}_{j,k+1/2}^{n} - \tilde{\mathbf{G}}_{j,k-1/2}^{n}],\end{aligned} \tag{31a}$$

where

$$\begin{aligned}\tilde{\mathbf{F}}_{j+1/2,k} &= \tfrac{1}{2}[\hat{\mathbf{F}}_{j+1,k} + \hat{\mathbf{F}}_{j,k} + \tilde{\mathbf{R}}_{j+1/2,k}\boldsymbol{\Phi}_{j+1/2,k}] \\ \tilde{\mathbf{G}}_{j,k+1/2} &= \tfrac{1}{2}[\hat{\mathbf{G}}_{j,k+1} + \hat{\mathbf{G}}_{j,k} + \hat{\mathbf{R}}_{j,k+1/2}\boldsymbol{\Phi}_{j,k+1/2}]\end{aligned} \tag{31b}$$

in which $\boldsymbol{\Phi}_{j+1/2,k}$ and $\boldsymbol{\Phi}_{j,k+1/2}$ are the dissipation terms in the x- and y-directions, respectively. In this study, $\phi = \frac{1}{2}$ is employed to get the second-order accuracy in time. The dissipation along the x-direction is

$$\begin{aligned}\boldsymbol{\Phi}_{j+1/2,k} = (&-|\boldsymbol{\Lambda}_{j+1/2,k}|\hat{\boldsymbol{\alpha}}_{j+1/2,k} + \boldsymbol{\Lambda}_{j+1/2,k}^{+}\boldsymbol{\varphi}^{+}\hat{\boldsymbol{\alpha}}_{j-1/2,k} \\ &- \boldsymbol{\Lambda}_{j+1/2,k}^{-}\boldsymbol{\varphi}^{-}\hat{\boldsymbol{\alpha}}_{j+3/2,k})\end{aligned} \tag{32}$$

$$\boldsymbol{\Lambda}_{j+1/2,k}^{\pm} = \operatorname{diag}\left\{\frac{a_{j+1/2,k}^{l} \pm |a_{j+1/2,k}^{l}|}{2}\right\} = \operatorname{diag}\{(a_{j+1/2,k}^{\pm})^{l}\}$$

$$\tilde{\boldsymbol{\Lambda}}_{j-1/2,k}^{+} = \operatorname{diag}\left\{\frac{1 + \operatorname{sgn}(a_{j+1/2,k}^{l})}{2}\, a_{j-1/2,k}^{l}\right\} = \operatorname{diag}\{(\tilde{a}_{j+1/2,k}^{+})^{l}\}$$

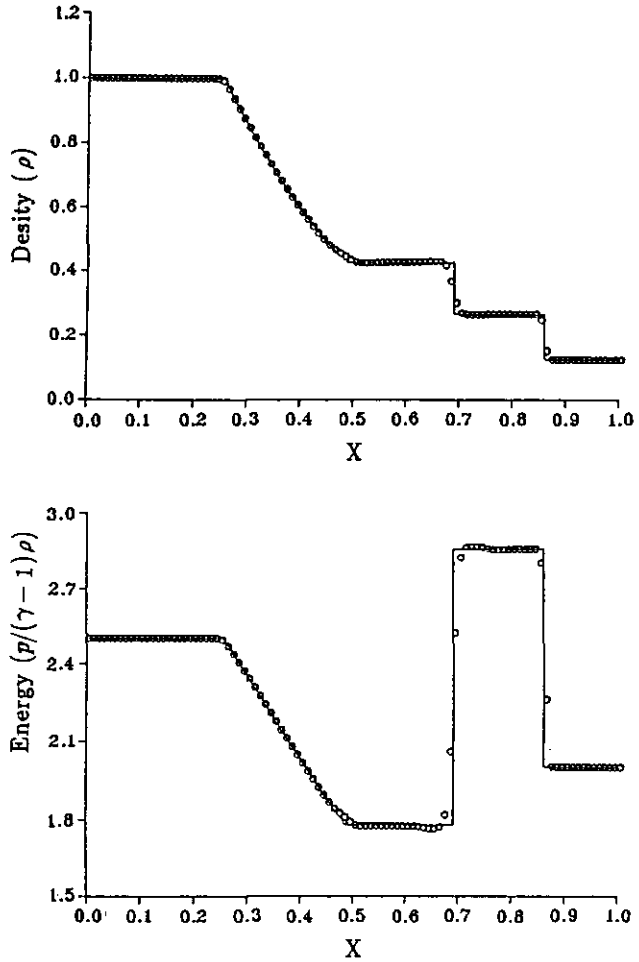

FIG. 7. (a) The resulting *density* contours of employing the superbee limiter to the Sod shock-tube problem, $\nu = 0.8$, $t = 0.2021$. (b) The resulting *energy* contours of employing the superbee limiter to the Sod shock-tube problem, $\nu = 0.8$, $t = 0.2021$.

$$\tilde{\Lambda}^{-}_{j+3/2,k} = \text{diag}\left\{\frac{1-\text{sgn}(a^l_{j+1/2,k})}{2}\, a^l_{j+3/2,k}\right\} = \text{diag}\{(\tilde{a}^{-}_{j+3/2,k})^l\}$$

$$\hat{\boldsymbol{\alpha}}_{j+1/2,k} = \frac{1}{J}\,\tilde{\mathbf{R}}^{-1}_{j+1/2,k}(\hat{\mathbf{U}}_{j+1,k} - \hat{\mathbf{U}}_{j,k}),$$

where $|\Lambda_{j+1/2,k}|$ is a diagonal matrix with element $|a^l_{j+1/2,k}|$'s and $\varphi^{\pm}$ are diagonal matrices with elements φ^l. Note that φ^l are similar to those specified in Eqs. (23), (26)–(28), provided that proper modifications are made. For example, $|\Delta u|_{\max}$ and $|\Delta u|_{\text{mean}}$ are modified to be the maximum and mean values of the components, $|a^l_{j+1/2,k}|_{\max}$ and $|a^l_{j+1/2,k}|_{\text{mean}}$, respectively, for all j and k. Here, we denote the slope ratios as

$$(r^{-}_{j+1/2,k})^l = \frac{\alpha^l_{j-1/2,k}}{\alpha^l_{j+1/2,k}}, \quad (r^{+}_{j+1/2,k})^l = \frac{\alpha^l_{j+3/2,k}}{\alpha^l_{j+1/2,k}}. \tag{33}$$

The expression of $\boldsymbol{\Phi}_{j,k+1/2}$ is similarly defined. $\hat{\mathbf{U}}_{j\pm1/2,k}$ and $\hat{\mathbf{U}}_{j,k\pm1/2}$ in the above equations are evaluated by Roe's average [18].

The implicit scheme of Eqs. (31)–(33) is solved by the following iterative method (similar to the Newton–Raphson method) so that both transient and steady-state calculations are suitable [1, 3, 21],

$$\begin{aligned}\delta\hat{\mathbf{U}}^q_{j,k} + \Delta t\,\phi[\delta^{\xi}(\hat{\mathbf{A}}^q_{j,k}\,\delta\hat{\mathbf{U}}^q_{j,k}) + \delta^{\eta}(\hat{\mathbf{B}}^q_{j,k}\,\delta\hat{\mathbf{U}}^q_{j,k})] \\ = \hat{\mathbf{U}}^n_{j,k} - \hat{\mathbf{U}}^q_{j,k} - \Delta t\,\phi[\delta^{\xi}\tilde{\mathbf{F}}^q_{j,k} + \delta^{\eta}\tilde{\mathbf{G}}^q_{j,k}] \\ - \Delta t\,(1-\phi)[\delta^{\xi}\tilde{\mathbf{F}}^n_{j,k} + \delta^{\eta}\tilde{\mathbf{G}}^n_{j,k}],\end{aligned} \tag{34}$$

where $\delta\hat{\mathbf{U}}^q_{j,k} = \hat{\mathbf{U}}^{q+1}_{j,k} - \hat{\mathbf{U}}^q_{j,k}$, $\delta^{\xi}\tilde{\mathbf{F}}^q_{j,k} = [\tilde{\mathbf{F}}^q_{j+1/2,k} - \tilde{\mathbf{F}}^q_{j-1/2,k}]$, $\delta^{\eta}\tilde{\mathbf{G}}^q_{j,k} = [\tilde{\mathbf{G}}^q_{j,k+1/2} - \tilde{\mathbf{G}}^q_{j,k-1/2}]$, etc. The superscript q is an index of subiteration. If the subiteration is converged, $\hat{\mathbf{U}}^q \sim \hat{\mathbf{U}}^{q+1} = \hat{\mathbf{U}}^{n+1}$. In order to apply the tri-diagonal solver of the system equation of the ADI (alternative direction implicit) method [21], the dissipations $\boldsymbol{\Phi}$ in $\tilde{\mathbf{F}}$ and $\tilde{\mathbf{G}}$ are properly interpreted so that the terms of $\delta^{\xi}(\cdot)$ and $\delta^{\eta}(\cdot)$ in the left-hand side of Eq. (34) become the first-order upwind differencing. After applying the linear-

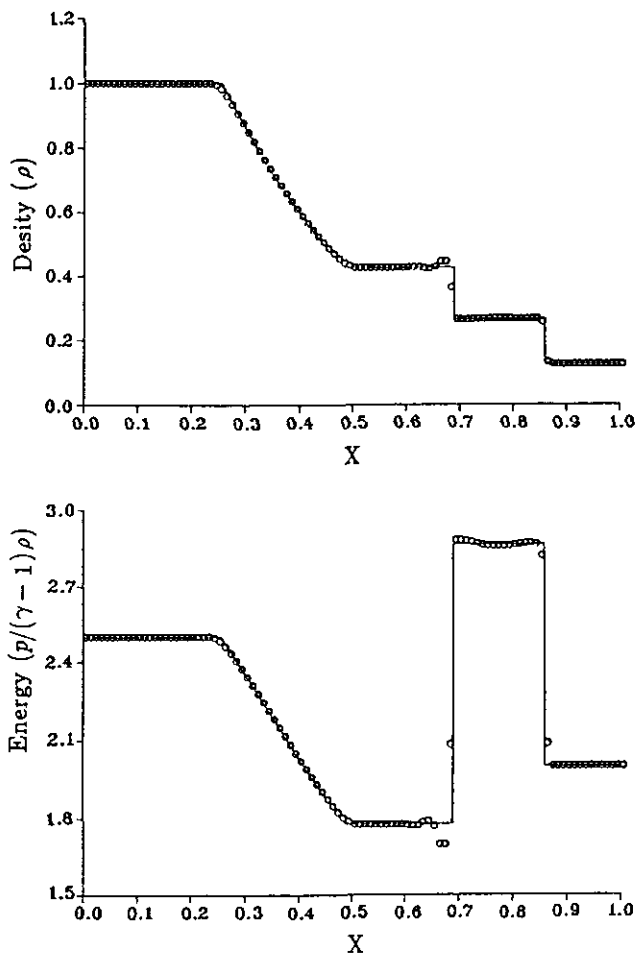

FIG. 8. (a) The resulting *density* contours of employing the proposed TVD scheme (Eqs. (23), (26), (28)) to the Sod shock-tube problem, $\nu = 0.8$, $t = 0.2021$. (b) The resulting *energy* contours of employing the proposed TVD scheme (Eqs. (23), (26), (28)) to the Sod shock-tube problem, $\nu = 0.8$, $t = 0.2021$.

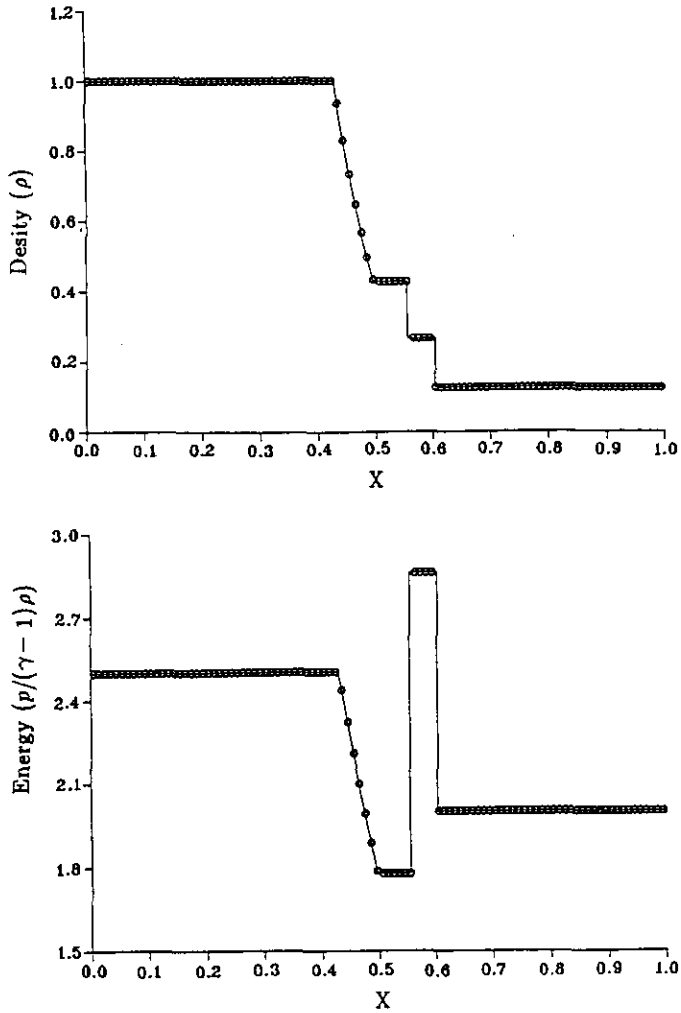

FIG. 9. (a) Density contours of the exact solution at $t = 0.0509$. (b) Energy contours of the exact solution at $t = 0.0509$.

ized conservative approximation and the ADI approximation to the implicit part, Eq. (34) takes the form [21]

$$[I + \Delta t\, \phi \mathbf{H}^{\xi}_{j+1/2,k} \cdot - \Delta t\, \phi \mathbf{H}^{\xi}_{j-1/2,k} \cdot]\mathbf{D}^* = \mathrm{RHS}$$

$$[I + \Delta t\, \phi \mathbf{H}^{\eta}_{j,k+1/2} \cdot - \Delta t\, \phi \mathbf{H}^{\eta}_{j,k-1/2} \cdot]\mathbf{D} = \mathbf{D}^* \qquad (35a)$$

$$\hat{\mathbf{U}}^{q+1} = \hat{\mathbf{U}}^q + \mathbf{D},$$

where

$$\mathbf{H}^{\xi}_{j+1/2,k} \cdot = \frac{1}{2}[(\hat{\mathbf{A}}_{j+1,k})^q + (\mathbf{\Omega}^{\xi}_{j+1/2,k})^q].$$

$$\mathbf{H}^{\eta}_{j,k+1/2} = \frac{1}{2}[(\hat{\mathbf{B}}_{j,k+1})^q + (\mathbf{\Omega}^{\eta}_{j,k+1/2})^q] \cdot \qquad (35b)$$

$$\mathbf{\Omega}^{\xi}_{j+1/2,k} = \mathrm{diag}(-\max(|a^l|))_{j+1/2,k}\, \Delta_{j+1/2}$$

$$\mathbf{\Omega}^{\eta}_{j,k+1/2} = \mathrm{diag}(-\max(|a^l|))_{j,k+1/2}\, \Delta_{k+1/2} \cdot$$

If the maximum residue is reduced by more than three orders of magnitude and at least three subiterations are computed, the loop of subiteration is stopped and goes to next time step.

RESULTS AND DISCUSSIONS

The first test problem employs the linear scalar equation

$$u_t + u_x = 0, \quad -1 \le x \le 1,$$
$$u(x, 0) = u^o(x), \qquad (36)$$

where $u^o(x)$ is a periodic function with a period of 2. The following three different initial conditions are to be considered

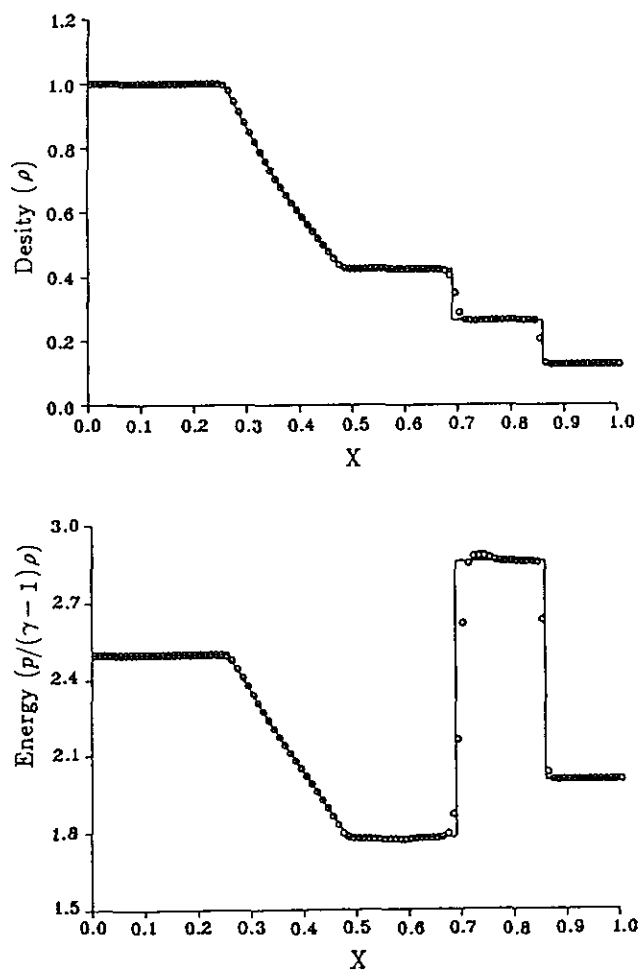

FIG. 10. (a) The resulting density contours of employing the superbee limiter to the Sod shock-tube problem, with initial conditions of Figs. 9a–b, $\nu = 0.8$, $t = 0.2021$. (b) The resulting energy contours of employing the superbee limiter to the Sod shock-tube problem, with initial conditions of Figs. 9a–b, $\nu = 0.8$, $t = 0.2021$.

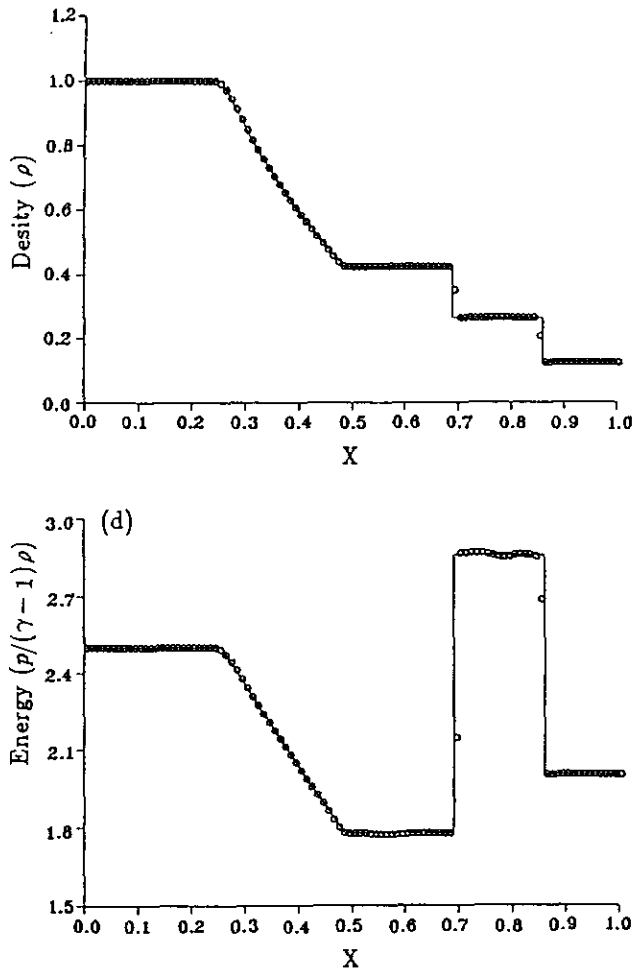

FIG. 11. (a) The resulting density contours of employing the proposed TVD scheme (Eqs. (23), (26), (28)) to the Sod shock-tube problem, with initial conditions of Figs. 9a–b, $\nu = 0.8$, $t = 0.2021$. (b) The resulting energy contours of employing the proposed TVD scheme (Eqs. (23), (26), (28)) to the Sod shock-tube problem, with initial conditions of Figs. 9a–b, $\nu = 0.8$, $t = 0.2021$.

(the first two are used in Ref. [22], and the third is used in Ref. [23]):

$$u^o(x) = 1, \quad |x| \le 0.2$$
$$= 0, \quad \text{otherwise} \tag{37a}$$

$$u^o(x) = \left[1 - \left(\frac{10x}{3}\right)^2\right]^{0.5}, \quad |x| < 0.3$$
$$= 0, \quad \text{otherwise} \tag{37b}$$

$$u^o(x) = -x \cdot \sin\left(\frac{3\pi x^2}{2}\right), \quad -1 \le x \le -\frac{1}{3},$$
$$= |\sin(2\pi x)|, \quad |x| < \tfrac{1}{3}$$
$$= 2x - 1 - \frac{\sin(3\pi x)}{6}, \quad \frac{1}{3} < x < 1. \tag{37c}$$

Figure 3a depicts the exact solution as well as the result of a TVD scheme (equipped with the superbee limiter) that employs the initial condition of Eq. (37a). For convenience, the numerical solutions in this study are illustrated by open circles, while the exact solutions are sketched using solid lines. An examination of this figure clearly indicates that the superbee limiter is not compressive enough to capture the linear discontinuity within two points. Figure 3b illustrates the results of the present TVD scheme equipped with the extremely compressive limiter of Eqs. (23)–(25), which is better than the associated solutions in Ref. [13]. Subsequent solutions, which employ different CFL numbers and/or employ the modified limiter (replacing Eqs. (24)–(25) with Eqs. (26)–(28)), also demonstrate the same result.

Figure 4a illustrates both the exact solution and the overcompressive result which employs the compressive limiter of Eq. (24) with the initial conditions of Eq. (37b). It should be noted that the superbee limiter gives a different type of overcompressed solution when used alone. If the third-order upwind TVD scheme (whose $\varphi = \text{Min}(\phi_l$ of Eq. (28), 2, $2r^-))$, which is similar to the Charkravarthy and Osher third-order upwind TVD scheme [24], is employed, discontinuities at the left and right corners are smeared as shown in Fig. 4b. After employing the modified limiter of Eqs. (26)–(28) (with $\nu =$

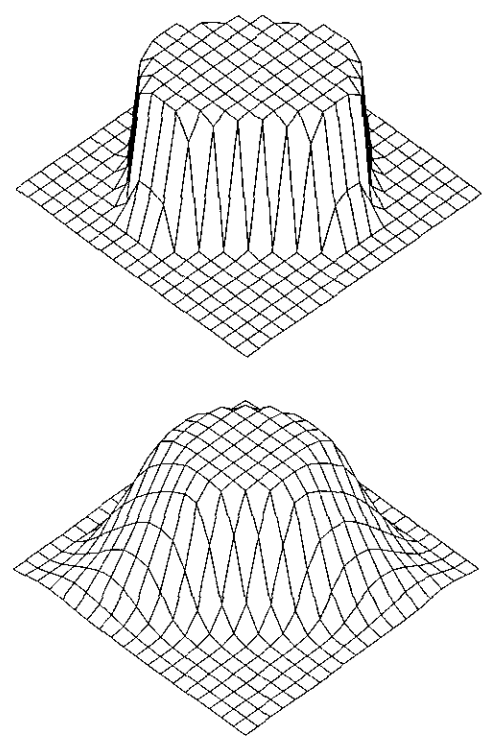

FIG. 12. (a) The resulting solution of employing the proposed limiter of Eqs. (23)–(25) to the two-dimensional scalar linear wave equation with initial conditions, Eqs. (33a)–(33b). (b) The resulting solution of employing the superbee limiter to the two-dimensional scalar linear wave equation with initial conditions, Eqs. (33a)–(33b).

0.5, $K = 1$, $\omega = 0.1$, and $\Delta\omega = 0.05$) and the extremum corrector, the overly compressed result, and the clipping effect at the extreme point do disappear (see Fig. 4c). Slightly more diffuse resolutions around the lower corners of Fig. 4c (as compared to Fig. 4a) are unavoidable side effects resulting from the release of the overcompressive character (because Eq. (27), instead of Eq. (26), is employed). The solution around the lower corners is better than that in Ref. [13], while the solution along two vertical lines is slightly worse than the solution of Ref. [13]. In this case, most of the solution is nearly identical with respect to the CFL number, except that the corners become slightly more diffuse as the CFL number takes a smaller value (see Fig. 4d with $\nu = 0.4$, for example).

The various solutions to the problem that results from using the third initial conditions all demonstrate similar characteristics and, thus, need not be compared. Solutions shown in Figs. 5a and b are the results of the wave after it has traveled to times $t = 2$ and 20 with $\nu = 0.8$ and 100 uniform points, respectively, where the solid lines are the exact solution. Note that these solutions are in complete agreement with each other, except that the extrema become slightly more smeared as the CFL number becomes smaller, and that they are clipped differently as the marching proceeds. Also note that the clipping effect can not be effectively deleted because, at the early stages, the employed extremum corrector identifies all the extreme points as extreme points around discontinuities. Consequently, the result is worse than that in Ref. [13].

The next test case employs the scalar nonlinear Burgers equation,

$$\begin{aligned} &u_t + uu_x = 0, \quad -1 \le x \le 1, \\ &t = 0, \quad u(0, x) = -\sin(\pi x) \\ &t > 0, \quad u(t, -1) = u(t, 1) = 0. \end{aligned} \tag{38}$$

Using a 40 uniform mesh and a CFL value of 0.8, the results just before and just after the formation of a shock are given in Figs. 6a and b, respectively. These figures clearly show that the nonlinear discontinuity, as well as the smooth region, are both captured very well. Figure 6c shows the result before the formation of the shock with a CFL value of 0.2, which demonstrates that a smaller CFL number has a slightly more diffusive result. As the shock is formed, the result is nearly insensitive to the CFL number. Since the CFL number has a similar effect on all the test cases, we will not discuss this effect below.

An example of the one-dimensional system equation problem is the Sod shock-tube problem [25], whose initial conditions are

$$\mathbf{U} = [\rho_L, u_L, p_L]^T = [1, 0, 1]^T, \quad \text{if } 0 \le x \le 0.5, \tag{39a}$$

$$= [\rho_R, u_R, p_R]^T = [0.125, 0, 1]^T, \quad \text{if } 0.5 \le x < 1. \tag{39b}$$

A uniform grid consisting of 100 uniform intervals was used. The numerical solutions were performed up to $t = 0.2$ with the CFL number taking the value of 0.8. The results of employing the superbee limiter are shown in Figs. 7a and b, while the results of employing Eqs. (23), (26)–(28) are shown in Figs. 8a and b. Compared with results of the superbee limiter, Figs. 8a–b show that, although the shock wave is resolved very well, postwave oscillation is found around the contact discontinuity wave. This is due to insufficient dissipation of the proposed adaptive limiter. Note that at the very beginning, the expansion wave, the contact surface, and the shock wave are close to each other and an adequate dissipation is required. For example, consider the exact solution at $t = 0.0509$ as the initial condition, where these waves are separated by a large enough number of grid points, as shown in Figs. 9a and b. The solution of the present limiter (Figs. 11a and b) resolves discontinuity very well, as can be seen by a comparison with those of the superbee limiter (see Figs. 10a and b). Therefore, it seems that further investigation on this issue is necessary.

The following problem is that of the two-dimensional scalar linear wave equation problem with a constant wave speed, $\mathbf{a} = \mathbf{i} + \mathbf{j}$. The initial conditions are

$$u_{i,j}^0 = 1, \quad \text{if } |x_{i,j} + y_{i,j}| \le \frac{\sqrt{2}}{2}, |x_{i,j} - y_{i,j}| \le \frac{\sqrt{2}}{2}, \tag{40a}$$

$$= 0, \quad \text{otherwise.} \tag{40b}$$

After computing for 800 steps with $\nu = 0.1$ and $\Delta x = \Delta y = 0.1$, the result of employing the limiter of Eqs. (23)–(25) (and also that of Eqs. (23), (26)–(28)) is shown in Fig. 12a. The result of employing the superbee limiter is shown in Fig. 12b. Since the present limiter is more compressive than the superbee limiter, the result of the former is better than that of the latter. However, for smooth initial conditions, the compressive character of both limiters compresses the solution to more and more blockwise distributions which are not shown here. In other words, the elements for constructing an adaptive TVD limiter for two-dimensional scalar equations should be shifted to those limiters with more diffusive characters.

Finally, the compressive TVD limiter is applied to an inviscid supersonic wind tunnel problem [26], whose result is shown in Fig. 13a. The problem begins with uniform Mach number 3 flow in an inviscid wind tunnel containing a step. The wind tunnel is 1 length unit wide and 3 length units long. The step is 0.2 length unit high and is located 0.6 length units from the left-hand end of the tunnel, and the tunnel is assumed to be two-dimensional. All the boundary conditions at the left are specified by inflow Dirichlet conditions, and at the right all the gradients are assumed to vanish. Initially, the wind tunnel is filled with a gamma-law gas with $\gamma = 1.4$, which everywhere has a density of 1.4, a pressure of 1.0, and a velocity of 3, and

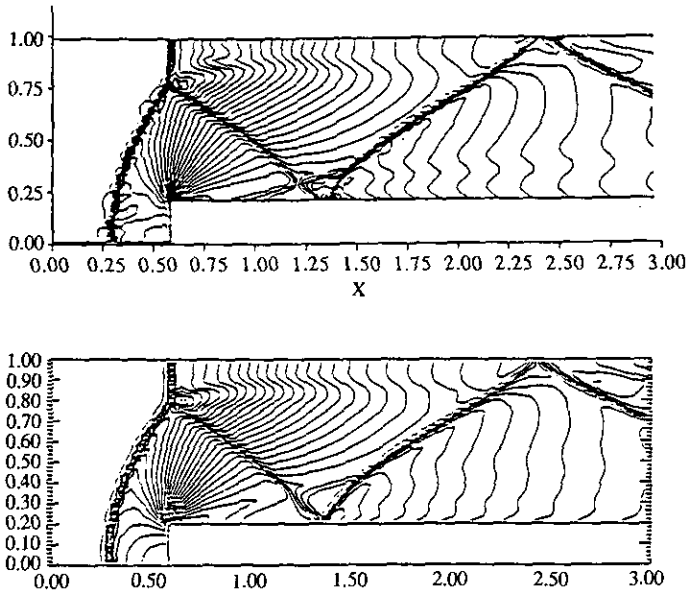

FIG. 13. (a) The resulting density contours of employing the implicit TVD scheme to the supersonic wind tunnel problem, $t = 4.0$, with $\nu_{max} = 2$, $\Delta\rho = 0.16$, and $0.4501 \leq \rho \leq 6.301$. (b) The PPM solution (density contours) at $t = 0.4$, Ref. [27].

is continuously fed from the left-hand boundary. Along the tunnel wall, reflecting boundary conditions are applied. The corner of the step is the center of a rarefaction fan and, hence, is a singular point. In the first four zones (the first row of cells just above the step) starting from the right of the corner of the step, the density values are reset so that their entropy values are equal to that in the cell just to the left and below the corner of the step. Note that the region of reset is smaller than the reset in Refs. [26, 27] because the Coakley splitting induces intrinsic dissipation.

Figure 13a is the result of the adaptive TVD limiter at $t = 4.0$ employing 121×41 uniform grid points ($\nu_{max} = 2$, $\omega_o = 0$, $\Delta\omega = 1$) and is comparable to the PPM solution of [26, 27] (Fig. 13b). The slip line is first slightly sharper than that in the PPM solution and then becomes slightly more smeared downstream. On the other hand, the oblique shock induced by the reattachment of the fluid turning around the corner of the step is stronger than that in the PPM solution.

In summary, it seems that the proposed adaptive limiter is suitable for the scalar one-dimensional hyperbolic conservation law. For cases governed by one-dimensional system equations, the limiter is a good scheme to resolve isolated discontinuities. For the two-dimensional scalar equation problems, as Roe pointed out [28], results for a two-dimensional problem deteriorate as the solution of the associated one-dimensional scalar equation problem improves. However, the result for a two-dimensional Euler equation problem is acceptable.

CONCLUSIONS

The TVD range of the explicit modified Lax–Wendroff scheme for scalar wave equations was revisited. The upper limit of the TVD range for a scalar linear wave equation is equal to the upper boundary of the monotonicity constraints of Roe and Baines. Subsequently, an adaptive TVD limiter, which is a combination of the third-order upwind TVD scheme and a compressive TVD limiter, was designed. Numerical tests proved that the proposed method resolves linear and nonlinear scalar discontinuity and smooth solution very well. An acceptable result is also found for a two-dimensional Euler equation problem. However, for the one-dimensional system equations and two-dimensional scalar equations cases further investigations are necessary.

REFERENCES

1. A. Harten, *J. Comput. Phys.* **49,** 357 (1983).
2. A. Harten, *SIAM J. Numer. Anal.* **21,** 1 (1983).
3. H. C. Yee, *Lecture Notes on a Class of High-Resolution Explicit and Implicit Shock-Capturing Methods, Von Karmann Institute for Fluid Dynamics Lecture Series 1989-04, March 6–10, 1989, Rhode-St-Genese, Belgium* (unpublished).
4. P. L. Roe, "Some Contributions to the Modelling of Discontinuous Flows," in *Proceedings, AMS-SIAM Sum. Sem. on Large-Scale Comp. in Fluid Mech., 1983,* edited by B. E. Engquist *et al.*, Lectures in Appl. Math., Vol. 22, Pt. 2 (Am. Math. Soc., Providence, RI, 1985), 63.
5. H. C. Yee, *J. Comput. Phys.* **68,** 151 (1987).
6. P. K. Sweby, *SIAM J. Numer. Anal.* **21,** 995 (1984).
7. P. L. Roe and M. J. Baines, "Algorithms for Advection and Shock Problems," in *Proceedings, 4th GAMM conference on Numerical Methods in Fluid Mechanics, 1982,* edited by H. Viviand p. 284.
8. P. L. Roe and M. J. Baines, "Asymmetric Behaviour of Some Non-linear Schemes for Linear Advection," in *Proceedings, 5th GAMM Conf. Num. Meth. in Fluid Mechanics, 1983,* edited by M. Pandolfi and R. Piva (Vieweg, Wiesbaden, 1984), p. 283.
9. T. J. Wu, Ph.D. dissertation, Institute of Aero. & Astro., National Cheng-Kung University Taiwan, 1991 (unpublished).
10. Y. N. Jeng, U. J. Payne, and T. J. Wu, "A Class of High Resolution TVD Schemes," in *Proceedings, 4th Natl. Conf. on Theor. & Appl. Mech., Chung Li, Taiwan, Dec. 14–15, STAMROC-14-L40, 1990* (unpublished).
11. Y. N. Jeng, U. J. Payne, and T. J. Wu, "On the Improvement of TVD Schemes by an Adaptive Limiter and an Extremum Discriminator," in *Proceedings, 8th Natl. Conf. on Mech. Eng. CSME, Taipei, Taiwan, Nov. 24, 1991,* p. 103 (unpublished).
12. A. Harten, *J. Comput. Phys.* **83,** 148 (1989).
13. C. W. Shu and S. Osher, *J. Comput. Phys.* **83,** 32 (1989).
14. B. P. Leonard, NASATM 100916 (ICOMP-88-11), NASA Lewis Research Center, 1988 (unpublished).
15. B. P. Leonard and H. S. Niknafs, *Comput. & Fluids* **19,** 141 (1991).
16. Y. N. Jeng and U. J. Payne, *J. Aircraft,* to appear.
17. P. L. Roe, "Fluctuations and Signals, a Framework for Numerical Evolution Problems," in *Numerical Methods for Fluid Dynamics,* edited by K. W. Morton and M. J. Baines (Academic Press, New York, 1982), p. 219.

18. P. L. Roe, *J. Comput. Phys.* **43,** 357 (1981).
19. T. J. Coakley, AIAA Paper No. 83-1958, 1983 (unpublished).
20. Y. N. Jeng and T. J. Wu, AIAA Paper No. 92-2627, 1992 (unpublished).
21. H. C. Yee and A. Harten, *AIAA J.* **25,** 266 (1987).
22. S. Zalesak, "A Preliminary Comparison of Modern Shock-Capturing Schemes: Linear Advection," in *Advances in Computer Methods for Partial Differential Equations, VI,* edited by R. Vichnevetsk and R. Stepleman (IMACS, New Brunswick, NJ, 1987).
23. A. Harten, B. Engquist, S. Osher, and S. Chakravarthy, *J. Comput. Phys.* **71,** 231 (1987).
24. S. R. Chakravarthy and S. Osher, AIAA Paper No. 85-0363, 1985 (unpublished).
25. G. A. Sod, *J. Comput. Phys.* **27,** 1 (1978).
26. P. R. Woodward and P. Colella, *J. Comput. Phys.* **54,** 115 (1984).
27. P. Colella and P. R. Woodward, *J. Comput. Phys.* **54,** 174 (1984).
28. P. L. Roe, *Numer. Methods Partial Differential Equations* **7** (1991), 277.